

Bi-directional Training for Composed Image Retrieval via Text Prompt Learning

Zheyuan Liu¹ Weixuan Sun¹ Yicong Hong¹ Damien Teney^{2,3} Stephen Gould¹

¹Australian National University

²Australian Institute for Machine Learning, University of Adelaide ³Idiap Research Institute

{zheyuan.liu, weixuan.sun, yicong.hong, stephen.gould}@anu.edu.au

damien.teney@idiap.ch

Abstract

Composed image retrieval searches for a target image based on a multi-modal user query comprised of a reference image and modification text describing the desired changes. Existing approaches to solving this challenging task learn a mapping from the (reference image, modification text)-pair to an image embedding that is then matched against a large image corpus. One area that has not yet been explored is the reverse direction, which asks the question, what reference image when modified as described by the text would produce the given target image? In this work we propose a bi-directional training scheme that leverages such reversed queries and can be applied to existing composed image retrieval architectures. To encode the bi-directional query we prepend a learnable token to the modification text that designates the direction of the query and then finetune the parameters of the text embedding module. We make no other changes to the network architecture. Experiments on two standard datasets show that our novel approach achieves improved performance over a baseline BLIP-based model that itself already achieves state-of-the-art performance.

1. Introduction

Composed Image Retrieval (CIR) [9, 21, 35] aims at retrieving images based on the user input of a reference image and a sentence stating certain desired changes. The retrieved target image must encompass the user-specified changes while remaining similar to the reference image on other aspects. Unlike conventional image [33] or text-based [19, 37] retrieval with one input modality, CIR is more precise, which is appreciated in domains such as image search or e-commercial product retrieval.

Existing approaches [2, 6, 8, 35] on CIR mostly focus on learning the mapping of embeddings from the given (reference image, text)-pair to a target image, where the multi-

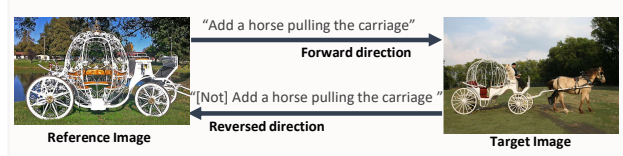


Figure 1. **Top:** (Forward direction) Existing methods on Composed Image Retrieval focus on mapping the input (reference image, modification text)-pair to the target image. **Bottom:** (Reversed direction) We propose to also exploit information in the mapping from the (target image, reversed modification text)-pair to the reference image. Note that the reversed text is an illustration, which we do not have and have to infer from existing data.

modal input pair is jointly embedded through various mechanisms including gating [35], multi-layer attention [6, 8] or convex summation [3]. However, few have considered the full potential of the information available in the training data. If we view conventional CIR methods as training in the forward direction from reference to target, while conditioning on the text; then it is easy to see that a reverse direction can be achieved from target to reference, provided that a suitable text reversal can be found (Figure 1). Harnessing information in such a bi-directional fashion benefits the training and increases the robustness of the model. We argue that this is particularly valuable given the limited dataset sizes [9, 21] and high annotation cost [27] of existing datasets for this task.

To this end, we propose bi-directional training for CIR to simultaneously learn to retrieve images (target or reference, respectively) from both the forward and reversed queries. As stated above, one major challenge is text reversal, that is, to create text that carries the opposite semantic meanings compared to the original. For human annotators, rewriting the text can be easy. However, with the absence of additional annotations, the naive approach of reversing text through, e.g., handcrafted linguistic rules can be diffi-

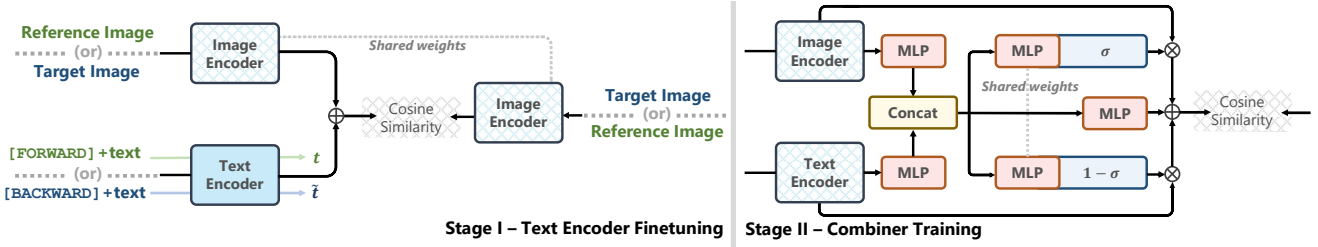


Figure 2. Our bi-directional training pipeline. Only modules of solid colors are being updated. Here, \otimes denotes element-wise product and \oplus denotes element-wise addition. Note the details of contrastive loss is not fully shown here (see Section 3.1), instead, we only illustrate with the positive target/reference images. **Left:** Text encoder finetuning, where we input queries of both directions (distinguished by colors), and infer \hat{t} through training, along with t . Note the bi-directional tokens prepended to the text. We omit the [CLS] token from the text encoder for brevity. **Right:** Combiner training detailing the architecture [4]. We train the model with bi-directional queries simultaneously, as in the previous stage.

cult. This is especially true for the CIR dataset on generic images, as the sentences are of great variations and high complexity. One approach is to pass the text embeddings through a dedicated module (e.g., an MLP) when inversion is needed, while preserving the rest of the joint embedding model and train end-to-end. We argue a better alternative is to leverage the text encoders of vision-and-language pre-trained (VLP) models, which are commonly used in CIR to extract text embeddings. The advantage of which is that such encoders are pretrained on massive corpus, and, hence, are powerful in capturing the nuanced semantics of natural language. Specifically, we take inspiration from recent work on few-shot text-guided image editing [26] and propose to prepend the text with special learnable tokens signifying its directionality. We then leverage the state-of-the-art two-stage training pipeline [4] of the combiner architecture [3], where the first stage is to finetune the text encoder. We discover that through finetuning, the text encoder can associate the concept of directionality of the text with the special text tokens, and generate different embeddings from the same text input. This allows us to effectively treat queries of both directions equally after finetuning, and make no further changes to the subsequent joint embedding model (i.e., the combiner) or its training process when we include the reversed queries.

In order to include the reversed queries in training, we involve a secondary loss term in the contrastive loss. To better take advantage of the reverse queries we employ a modified sampling strategy for negative samples, such that the loss is more coherent in the bi-directional training scheme. We refer readers to Section 3.1 for details.

In summary, we propose a bi-directional training scheme for Composed Image Retrieval (CIR), which jointly trains on the forward queries, i.e., from reference to target images, as well as the reversed queries from target to reference. To obtain text embeddings of reversed semantics, we prepend the text with learnable tokens and finetune the text encoders.

Additionally, we modify the contrastive loss on the reversed path. No further changes to the model architecture or training pipeline are needed, which makes our approach easily applicable to existing methods. We empirically show that our approach achieves improved performance on datasets of diverse domains over a BLIP-based baseline that has already achieved state-of-the-art performance.

2. Related Work

Composed Image Retrieval. The task of Composed Image Retrieval (CIR) introduced by Vo et al. [35] aims at studying the composition of multi-modal features, where initially inputs of low complexity [11, 13] are considered. It is later adopted for fashion product [5, 9, 10], and recently further extend into generic images [21].

Most existing methods follow a fusion paradigm, where the features of the input reference image and text are jointly embedded and compared against features of all candidate target images for the closest match. Extensive research [2, 3, 6, 8, 21, 35] is done on the fusion mechanism of the network, with the most recent state-of-the-art [3, 4] adopting a combiner architecture that performs a convex combination of the input modalities within the CLIP [25] feature manifold. We note that this is the first method that simultaneously achieves state-of-the-art on both fashion and generic image datasets. Concurrently, others have explored splitting CIR into two-stage with coarse and fine searching [36], disentangling the image-image and image-text matching into dual branches [7], and expanding the task into zero-shot scenarios [27].

Among methods developed for CIR, we are mostly related to DCNet [14], where a Correction Module is used to model the difference between the reference and target images and match it to the text. In other words, it explores a different directionality of the training data than ours. Compared to DCNet, our method does not require an additional

module, or joint loss that connects the said module to the main network. Instead, our bi-directional training treats samples of both directions in the same manner. We also avoid computing feature differences through subtractions, which previous work [1] suggests can be hard to learn.

Cycle consistency. Our bi-directional training resembles the cycle-consistency concept seen in vision-and-language (e.g., Robust VQA [30]) and generation tasks (e.g., CycleGAN [39]), as we share the philosophy of manipulating model inputs and outputs to further exploit information in the training instances. However, such a concept bears different motivations and designs under various task setups. For VQA, it is implemented as a secondary question-answering stage with generated rephrases of the question, which improves the robustness of the model under linguistic variations. CycleGAN, however, utilizes cycle consistency with the absence of paired training instances between two domains. We note that CIR is different in that, three entities are included in the input and output. This setup requires unique designs, hence, making our method fundamentally different from previous work.

Finetuning on Text Prompt. Recent work on few-shot text-guided image editing has demonstrated the potential of special tokens in pre-trained text encoders. Specifically, Ruiz et al. [26] show that through finetuning, it is possible to bind the appearances of a certain instance in an image with artificially injected special tokens within the text prompt, so that the model can generate diverse samples containing said instance. Though not entirely equivalent, we take inspiration from the above work and adopt a similar idea in finetuning the text encoder. Our intention is to associate the concept of text directionality with special tokens, so that the model can recognize the need of reversing the semantics of the language when needed.

3. Bi-directional Composed Image Retrieval

Given the embeddings of a query of (reference image, modification text)-pair denoted as $q = (I_R, t)$, the objective is to locate a target image that best matches the query, whose embedding is denoted as I_T . Our goal is to also learn on the reversed query $\tilde{q} = (I_T, \tilde{t})$ simultaneously, which maps from the target I_T to the I_R . Here, \tilde{t} represents the text embedding that is semantically reversed. However, \tilde{t} is not directly computable as the text associated with such reversed embeddings do not exist in the training data. To overcome this difficulty we propose to infer the semantically reversed text embedding \tilde{t} from the original modification text using the text encoder, as detailed below.

3.1. Bi-directional Training

Text Prompt Learning. As shown in Figure 2 (left), we infer \tilde{t} through the finetuning of the text encoder, such that

it can produce text embedding of either direction for a given text. Specifically, we prepend special learnable tokens to the modification text sentences. The idea is to bind the concept of query directionality to such tokens through learning.

Here one option is to make no changes to the text of the forward queries, and only inject a token for when the text needs to be reversed. The implication is that the forward queries shall be trained in their de-facto forms (see Section 3.2), while only making necessary changes to the additional augmentations included. However, this introduces an asymmetry in the treatment of the forward and reversed queries. Our intuition is that the balanced approach will force the model to better recognize the purpose of the injected tokens and distinguish between the forward and reversed modes.

We choose [FORWARD] and [BACKWARD] as the learnable tokens for the forward and reversed queries respectively in all our experiments. Together with the [CLS] token from the text encoder, which is pretrained to summarize the text, a tokenized text sequence t of $\{t_1 \dots t_n\}$ in the forward query is then processed into $\{[CLS], [FORWARD], t_1 \dots t_n\}$, which is passed to the text encoder for embedding. Likewise for the reversed case.

We note that prompt design [17, 26] could potentially be of significant value to the end results. However, our focus is on the bi-directional training scheme, hence, we choose to rely on simple, generic tokens and make no specific adjustments to suit each dataset.

Modifications to the Training Pipeline. A favorable characteristic of our approach is the minimum changes made to the existing training pipeline. Here, we leverage the state-of-the-art two-stage training scheme (details of which are in Section 3.2), as illustrated in Figure 2. We note that, after finetuning the text encoder to infer \tilde{t} , the reversed queries $((I_T, \tilde{t}), I_R)$ can be constructed by a simple exchange of image orders. The entire process is computed on-the-fly with low additional cost. We then treat all queries equally regardless of their directionality, which allows us to train the second-stage combiner with bi-directional samples simultaneously without make any change to its architecture.

Negative Sampling in Contrastive Loss. We follow previous work and use the batch-based classification (BBC) loss [35]. Given a batch size of B , with the embeddings of the i -th query pair (I_R^i, t^i) , its corresponding positive target I_T^i , the forward query loss is computed as:

$$\mathcal{L}_F = -\frac{1}{B} \sum_{i=1}^B \log \left[\frac{\exp \left[\lambda \cdot \kappa \left(f(I_R^i, t^i), I_T^i \right) \right]}{\sum_{j=1}^B \exp \left[\lambda \cdot \kappa \left(f(I_R^i, t^i), I_T^j \right) \right]} \right], \quad (1)$$

where $f(\cdot, \cdot)$ denotes the combination function, $\kappa(\cdot, \cdot)$ is the similarity kernel implemented as cosine similarity and λ is

the temperature parameter. We follow Baldrati et al. [4] and set λ to 100 in all our experiments. As the denominator shows, we normalize over all other matches within a batch in training, which includes both the positive I_T^i and all other target images in the batch as negatives I_T^j for $j \neq i$.

When training on the reversed queries that maps query (I_T, \tilde{t}) to reference image I_R , multiple options exist in sampling the negatives to form a contrastive loss. Here, we propose to formulate the loss as:

$$\mathcal{L}_B = -\frac{1}{B} \sum_{i=1}^B \log \left[\frac{\exp \left[\lambda \cdot \kappa \left(f(I_T^i, \tilde{t}^i), I_R^i \right) \right]}{\sum_{j=1}^B \exp \left[\lambda \cdot \kappa \left(f(I_T^j, \tilde{t}^i), I_R^i \right) \right]} \right] \quad (2)$$

where we have chosen to sample the negatives among candidate target images, i.e., I_T^j , as in Equation 1. Our intuition is to unify losses for the forward and reversed queries so that they are learned to contrast against the same group of negatives. We empirically confirm that such a loss obtains better performance compared to, e.g., sampling negatives among the I_R^j (see Section 4.3).

The loss for bi-directional training is then computed as the weighted sum of losses for forward and reversed queries,

$$\mathcal{L} = \mathcal{L}_F + \alpha \mathcal{L}_B, \quad (3)$$

where α is a hyperparameter to balance the magnitudes of the two loss terms. We refer readers to the supplementary material for details on determining this parameter.

3.2. Model Architecture and Training Pipeline

We base our bi-directional training on a state-of-the-art baseline obtained using the combiner architecture [3, 4] with BLIP [18] vision-and-language pretrained (VLP) model, termed BLIP4CIR. We follow Baldrati et al. [4] and adopt a two-stage training scheme, detailed as follows.

Text Encoder Finetuning. As shown in Figure 2 (left), we first finetune the text encoder. The architecture is relatively light with the multi-modal combination done through an element-wise addition. The output is compared against embeddings of candidate targets through cosine similarity. Note that the image encoder is kept frozen as it is prohibitively expensive to finetune.

The intuition of this finetuning stage is to reduce the domain gap between the pretraining tasks and the downstream task, CIR. The element-wise addition is used to encourage the output t as displacement vectors between I_R and I_T in the image manifold. Once the text encoder is finetuned, we freeze it and train a combiner module that replaces the element-wise addition mentioned above, which involves more sophisticated joint embedding functions.

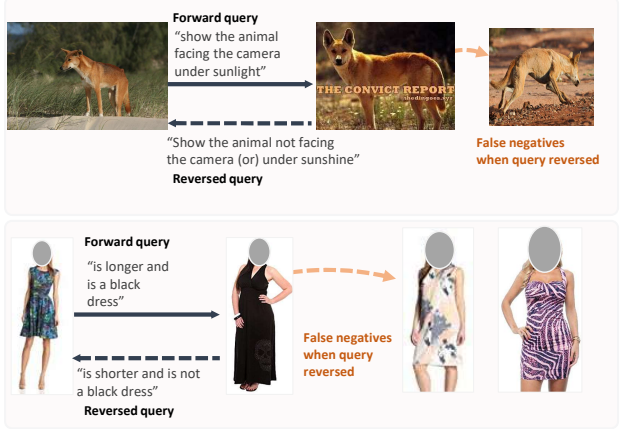


Figure 3. False negatives can exist in the reversed direction. A one-to-one text in the forward direction can become one-to-many when its semantics are reversed. Since we lack human labels for the reversed queries, only the original reference image is deemed positive. We point out that this issue is related to both the semantics of the text, as well as the image corpus. Hence, the prevalence of false negatives might vary for individual samples in different datasets. Note that the reversed text here is provided to illustrate the case, we do not have such annotations in the datasets.

Combiner Training. In the second-stage training, combiner replaces element-wise addition as the joint embedding function, with architecture depicted in Figure 2 (right). We refer readers to the original paper [3] for details. Overall, it can be viewed as a three-branch summation, with two branches implemented as a convex combination of the two input modalities, and a third branch of a learned image-text mixture. Note that the output of the combiner is forced to be similar to the raw image embeddings from the image encoder, while no additional projection or normalization is applied to the output of the image encoder. We find this detail vital to the high performance and quick convergence of the architecture.

BLIP Embeddings. We propose to change the CLIP [25] image and text encoders in both stages to BLIP [18]. The motivation is two-fold. First, BLIP has been demonstrated to be a powerful VLP network, and through early experiments, we found its text encoder to be better than CLIP’s. Second, we notice that BLIP is trained on text of higher complexity that better matches the annotations in CIR datasets. In contrast, CLIP is only trained on simple image-level labels prepended with a fixed prompt (e.g., “An image of [noun]”) [25]. We hypothesize that the BLIP text encoder is of stronger reasoning ability, and is, therefore, better suited to CIR. This is especially true for bi-directional training, as the text encoder needs to reverse the semantics of a given sentence. We also note that the choice of image encoder for CIR must take into account the large do-

main gap between the fashion and generic images, as previous work [21] discovers that VLP models trained only on generic images (e.g., OSCAR [20]) performs poorly on Fashion datasets. To compare, CLIP and BLIP are both trained on datasets of very large scale. While the training data of CLIP is proprietary, Li et al. [18] state that BLIP is trained on LAION [29], which contains 115M of filtered image-text pairs of diverse contents. We empirically confirm that BLIP provides a much stronger baseline over the stock CLIP encoders.

The change from CLIP to BLIP encoders is straightforward, as they are of similar Transformer [34] structures. Note that we do not involve the cross-attention fusion layer in BLIP that jointly embeds image and text modalities. Instead, we treat the image and text encoders as separate modules, as shown in Figure 2. This is to align with the usage of CLIP so that we can preserve the stock training pipeline. We use the default [CLS] token to summarize the text [18].

3.3. False Negatives in Reversed Queries

A systematic issue for our bi-direction training scheme is the occurrences of false negatives in the reversed queries. As illustrated in Figure 3, a one-to-one modification text in the forward query could become one-to-many when its semantics are reversed. For instance, a text of “*change to a white cat*” will be reversed to “*change from a white cat*”, which now leads to all cats (black, gray, ginger, fawn, etc.) that are not white — yet, only one image (i.e., the one in the original reference image) is labeled as the positive. We especially note that the prevalence of false negatives in the reversed path is related to the semantics of the text as well as the image corpus (e.g., following the example above, the number cat images in the corpus shall affect the number of false negatives). Hence, the scale of such an issue can vary for individual samples across datasets. This renders global label smoothing techniques [32] ineffective in our testings, as it could inadvertently affect queries with few false negatives and hurt the performance.

Granted, false negatives also exist in the forward path [9, 21], due to the prohibitive high cost in exhaustively labeling all candidates for each query. But they are less common, as human annotations are often sufficiently specific. Plus, existing metrics are designed to mitigate the issue by using Recall@ K of large K values.

We argue that nevertheless, training on the reversed queries still benefits the model, as demonstrated by our experiments of improved performance. However, special attention shall be paid in balancing the magnitudes of the loss terms (Equation 3), as the loss of the reversed path is generally higher. We also note that the prevalence of false negatives in the reversed direction suggests that validating on such reversed queries will lead to inferior results (see supplementary material for details).

Inference Strategy. Following the above, we design our inference strategy mirroring existing work [4, 35], which only performs on the forward queries. For each query, we rank the similarities of the combined (I_R, t) embedding with all candidate I'_T and pick the highest as the prediction.

4. Experiments and Discussions

Datasets and Metrics. We follow Baldrati et al. [4] and test on two datasets of different domains.

Fashion-IQ [9] focuses on fashion products of three subtypes, *Dress*, *Shirt* and *Toptee*. In total it contains over 30k triplets sampled from 77k images. Each triplet includes two human-generated annotations. We follow previous work and report Recall@ K with $K = 10$ and 50, while comparing the overall model performance with $(R@10 + R@50)/2$, as advised by Guo et al. [9]. The choice of K accounts for the potential false negatives in the forward queries. All results are on the validation set, as the test set is not publicly available.

CIRR [21] includes around 36k triplets sampled from 21k generic images sourced from NLVR² [31]. The human annotations are of higher complexity compared to Fashion-IQ. The dataset is designed to overcome the issue of false negatives, as it is prohibitive to exhaustively label every candidate target for each input query. Specifically, Liu et al. [21] group images by subsets of six and draw reference-target pairs from them. When annotating a given pair, annotators are instructed to avoid creating false negatives within the subset from which the pair is drawn. To this end, the evaluation protocol for CIRR is designed to be a combination of standard Recall@ K with $K = 1, 5, 10, 50$ and Recall_{Subset}@ K with $K = 1, 2, 3$, where Recall_{Subset}@ K only considers candidates from the same subset as the pair. Following Liu et al. [21], we assess the overall model performance with $(R@5 + R_{Subset}@1)/2$. Results in the main table are reported on the test set, the ground truths of which are not available. Instead, we obtain results through the official evaluation server¹. Results of ablation studies are reported on the validation set.

Implementation Details. We adopt the default image pre-processing scheme and model configuration as in [4], except when BLIP encoders [18] require a different setting in dimensions. This includes the input image resolutions (384 × 384) and the combiner input feature dimension (256 from BLIP encoder outputs).

For finetuning the text encoder, we follow BLIP downstream task settings and optimize with AdamW [22] for 15 epochs, with a learning rate of 5×10^{-5} , a weight decay of 0.05 and a cosine learning rate schedule. We increase the learning rate of the last linear projection layer to 5×10^{-3} to speed up the convergence. For training the combiner, we

¹<https://cirr.cecs.anu.edu.au/>

Methods	Dress		Shirt		Toptee		Average		Avg. Metric	
	R@10	R@50	R@10	R@50	R@10	R@50	R@10	R@50		
1	MRN [15]	12.32	32.18	15.88	34.33	18.11	36.33	15.44	34.28	24.86
2	FiLM [24]	14.23	33.34	15.04	34.09	17.30	37.68	15.52	35.04	25.28
3	TIRG [35]	14.87	34.66	18.26	37.89	19.08	39.62	17.40	37.39	27.40
4	Relationship [28]	15.44	38.08	18.33	38.63	21.10	44.77	18.29	40.49	29.39
5	CIRPLANT [21]	14.38	34.66	13.64	33.56	16.44	38.34	14.82	35.52	25.17
6	CIRPLANT w/OSCAR [21]	17.45	40.41	17.53	38.81	21.64	45.38	18.87	41.53	30.20
7	VAL w/GloVe [6]	22.53	44.00	22.38	44.15	27.53	51.68	24.15	46.61	35.40
8	CurlingNet [36]	24.44	47.69	18.59	40.57	25.19	49.66	22.74	45.97	34.36
9	DCNet [14]	28.95	56.07	23.95	47.30	30.44	58.29	27.78	53.89	40.84
10	CoSMo [16]	25.64	50.30	24.90	49.18	29.21	57.46	26.58	52.31	39.45
11	MAAF [8]	23.8	48.6	21.3	44.2	27.9	53.6	24.3	48.8	36.6
12	ARTEMIS [7]	25.68	51.25	28.59	55.06	21.57	44.13	25.25	50.08	37.67
13	SAC w/BERT [12]	26.52	51.01	28.02	51.86	32.70	61.23	29.08	54.70	41.89
14	AMC [38]	31.73	59.25	30.67	59.08	36.21	66.06	32.87	61.64	47.25
15	CLIP4CIR [4]	33.81	59.40	39.99	60.45	41.41	65.37	38.32	61.74	50.03
16	BLIP4CIR (first-stage)	37.13	62.67	35.92	60.40	43.60	68.28	38.88	63.78	51.33
17	BLIP4CIR	40.65	66.34	40.38	64.13	46.86	69.91	42.63	66.79	54.71
18	BLIP4CIR+Bi (first-stage)	36.94	63.71	37.49	60.06	43.60	67.77	39.34	63.85	51.60
19	BLIP4CIR+Bi	42.09	67.33	41.76	64.28	46.61	70.32	43.49	67.31	55.40

Table 1. Comparison on Fashion-IQ validation set, we follow Guo et al. [9] to report Average Metric as $(R@10+R@50)/2$. Best (resp. second-best) numbers are in bold-black (resp. blue), this excludes intermediate first-stage text encoder fine-tuning results marked in gray (rows 16, 18). BILP4CIR denotes the baseline using BLIP encoders. +Bi denotes the bi-directional training. For CLIP4CIR [4], we report their best-performing model that uses the two-stage training with RN50x4 as backbone. Rows 1-2 are cited from [9].

Methods	Recall@K				Recall _{Subset} @K			Avg. Metric	
	K = 1	K = 5	K = 10	K = 50	K = 1	K = 2	K = 3		
1	TIRG [35]	14.61	48.37	64.08	90.03	22.67	44.97	65.14	35.52
2	TIRG+LastConv [35]	11.04	35.68	51.27	83.29	23.82	45.65	64.55	29.75
3	MAAF [8]	10.31	33.03	48.30	80.06	21.05	41.81	61.60	27.04
4	MAAF+BERT [8]	10.12	33.10	48.01	80.57	22.04	42.41	62.14	27.57
5	MAAF-IT [8]	9.90	32.86	48.83	80.27	21.17	42.04	60.91	27.02
6	MAAF-RP [8]	10.22	33.32	48.68	81.84	21.41	42.17	61.60	27.37
7	CIRPLANT [21]	15.18	43.36	60.48	87.64	33.81	56.99	75.40	38.59
8	CIRPLANT w/OSCAR [21]	19.55	52.55	68.39	92.38	39.20	63.03	79.49	45.88
9	ARTEMIS [7]	16.96	46.10	61.31	87.73	39.99	62.20	75.67	43.05
10	CLIP4CIR [4]	38.53	69.98	81.86	95.93	68.19	85.64	94.17	69.09
11	BLIP4CIR (first-stage)	35.18	67.11	79.18	94.70	68.71	86.65	94.51	67.90
12	BLIP4CIR	40.17	71.81	83.18	95.69	72.34	88.70	95.23	72.07
13	BLIP4CIR+Bi (first-stage)	35.30	67.42	79.88	94.58	68.55	86.46	94.75	67.99
14	BLIP4CIR+Bi	40.15	73.08	83.88	96.27	72.10	88.27	95.93	72.59

Table 2. Comparison on CIRR test set. We follow Liu et al. [21] and report the Average Metric as $(\text{Recall}@5+\text{Recall}_{\text{Subset}}@1)/2$. Best (resp. second-best) numbers are in bold-black (resp. blue), this excludes intermediate first-stage text encoder fine-tuning results marked in gray (rows 11, 13). BILP4CIR denotes the baseline using BLIP encoders. +Bi denotes the bi-directional training. For CLIP4CIR [4], we report their best-performing model that uses the two-stage training with RN50x4 as backbone. Rows 1-8 are cited from [21].

adopt the original settings detailed in [3] and train for 200 epochs. The batch size of baseline experiments (i.e., without bi-directional training) follows [4]. The batch size of all bi-directional training experiments is reduced by half due to the GPU memory limit.

All experiments are trained with mixed-precision [23] in PyTorch with one NVIDIA A100. We base our implementation on the official codebases released by Baldrati et al. [4]² and Li et al. [18]³.

²<https://github.com/ABaldrati/CLIP4Cir>

³<https://github.com/salesforce/BLIP>

4.1. Results on Fashion-IQ

Table 1 shows the performance comparison between our approach and existing state-of-the-art methods on Fashion-IQ. We note that our BLIP-based baseline model (row 17) outperforms all previous approaches by a large margin. Impressively, through the first-stage text encoder finetuning (row 16), the performance already surpasses the previous best-performing model based on CLIP (row 15), demonstrating the high quality of BLIP embeddings. With the addition of bi-directional training, the overall performance

Methods	Neg-Sampling	Bi-Token	Fashion-IQ			CIRR			
			R@10	R@50	Average	R@1	R@5	R _{Subset} @1	Average
1 BLIP4CIR	—	—	42.63	66.79	54.71	41.11	74.89	72.66	73.78
2 BLIP4CIR+Bi	○	—	42.43	67.23	54.83	40.61	74.46	73.36	73.91
3 BLIP4CIR+Bi	—	○	43.30	66.77	55.03	40.28	73.95	72.57	73.26
4 BLIP4CIR+Bi	FULLY-CONFIGURED	—	43.49	67.31	55.40	42.36	75.46	72.90	74.18

Table 3. Ablation studies on Fashion-IQ and CIRR. Best numbers are in bold. Results reported on validation sets. For Fashion-IQ, we report the average Recall@10 and 50 of all three categories. For CIRR, the Average column denotes $(\text{Recall}@5 + \text{Recall}_{\text{Subset}}@1)/2$, as in Table 2. *Bi-Token* suggests adding learnable tokens to queries of both directions (i.e., bi-directional). *Neg-Sampling* represents our negative sampling scheme in the reversed contrastive loss. Here ○ denotes the item we are ablating (i.e., where we remove this particular item from the fully-configured model and assess the outcome).

is further improved consistently throughout the two stages (rows 16 v.s. 18; rows 17 v.s. 19). On the final results obtained in the second stage, we gain notable improvements on categories of *Dress* and *Shirt*, while retaining approximately a similar performance on *Toptee* compared to the baseline. We conjecture that each sub-class of data might benefit from the bi-directional training differently, due to the quality of the reversed queries considering the issue of false negatives and the specific image corpus (see Section 3.3).

4.2. Results on CIRR

Table 2 compares the performance of state-of-the-art methods with our approach on CIRR test set. We note that BLIP (row 12) brings a consistent performance increase compared to the previous best (row 10), as in Fashion-IQ. Our bi-directional training scheme (row 14) brings further increase to the performance of the strong baseline. Admittedly, the performance increase is inconsistent across metrics, particularly for $\text{Recall}_{\text{Subset}}@K$. We conjecture two reasons that could account for this. First, the high complexity of the text in CIRR would render the learning of the reversed semantics harder. Second, we notice that the combiner gains very little, if none, on $\text{Recall}_{\text{Subset}}@K$ throughout training, and that the fluctuations in performance are high among epochs. Given that $\text{Recall}_{\text{Subset}}@K$ is both more challenging by design and of high granularity (as it only considers five candidates from the same image subset [21]), we point out the possibility that the state-of-the-art combiner architecture, though powerful, may fail in this metric; and that the performance difference in $\text{Recall}_{\text{Subset}}@K$ between our method and the baseline may merely be caused by the fluctuations mentioned above. We refer readers to the supplementary material for further analysis on this subject.

For $\text{Recall}@K$, our method gains noticeable improvements when $K = 5$ and onwards, suggesting that valuable information exists in the reversed queries that help the model. For $\text{Recall}@1$, we obtain a similar performance as the baseline. Given that $\text{Recall}@1$ could potentially be

impacted by false negatives in the forward queries [21], and that the dataset recommends an assessment metric that instead includes $\text{Recall}@5$, we conclude that our bi-directional training is generally beneficial to this task.

4.3. Ablation Studies

We conduct ablation studies on the two design choices of our method detailed in Section 3.1, as shown in Table 3.

Negative Sampling in Reversed Contrastive Loss. In row 2, we compare the negative sampling scheme in the reversed path. Here, we report results obtained by contrasting against I_R^j as opposed to I_T^j in Equation 2. We note that the proposed sampling scheme is vital to the bi-directional training on both datasets. Specifically, we find that if adopting the negative sampling scheme on I_R^j , the model gains very little from the bi-directional training, with $\text{Recall}@K$ either dropping below the baseline (row 1) or merely slightly improving over it. We conjecture that a negative sampling scheme on I_R^j in the reverse queries causes a misalignment between the forward and reversed training paths, as the model is trained to contrast against I_T^j in the forward queries. To compare, our proposed sampling technique is more coherent and yields better performance. We note that the $\text{Recall}_{\text{Subset}}@1$ for CIRR presents as an outlier in this case. In this particular case, we propose to assess the performance difference more on the global Recall metrics, and refer to our discussions on the granularity of $\text{Recall}_{\text{Subset}}$ as well as the general learning behavior of the baseline method in Section 4.2.

Bi-directional Text Tokens. Table 3 row 3 demonstrates the effectiveness of involving learnable tokens in both directions of the text. Interestingly, we discover that compared to Fashion-IQ, CIRR is more benefited from such a technique. Without it, the performance, in particular on $\text{Recall}@5$, drops below baseline (row 3 v.s. 1). The reason is thought to be the complexity of the text inputs. In Fashion-IQ, the text is often short and carries simple meanings (see Figure 4 h-k) e.g., “longer sleeves” or “make the dress black”. In such cases, prepending a token solely in



Figure 4. Qualitative examples obtained with our method. In each example, gray box (leftmost) denotes the reference image, green box denotes the positive target, modification text is provided above the images. We show the top-5 candidates in ranking, except for when the positive target is ranked beyond top-5, in which case we remove the fifth-ranked candidate and append the positive at the end. This includes examples (b), (j) and (k). Examples (a-e) obtained from CIRR, (h-k) obtained from Fashion-IQ.

the reversed direction might still result in a proper reversion in semantics — as the model could learn to associate the token with “not”. However, the same cannot be said for CIRR, where text tends to be more complicated [21], as shown in Figure 4 (a-e). In such scenarios, our more balanced approach can better assist the model in identifying the directionality and associating it with said tokens.

4.4. Qualitative Examples

Figure 4 illustrates the qualitative examples of the retrieved results on both datasets. We specifically demonstrate successful cases where positive targets are highly ranked (d, e, h), as well as failure cases (b, j, k). We especially point to (d) and (e), where our method succeeds in reasoning over text with sophisticated intentions and retrieving the target, which demonstrates the quality of the BLIP embeddings as well as the power of our method.

As discussed in Section 3.3, we expect to encounter the issue of false negatives when reversing the queries. We show that for generic, short descriptions commonly found in Fashion-IQ (h-k), the reversed text can be widely imprecise, thus, leading to a great many possible candidates. The issue is worsened as images within Fashion-IQ can be of high similarity (e.g., j) — partially due to the natural low variability of cloth images. We show that this issue is less

noticeable in CIRR, as the images are often diverse, containing multiple entities and/or rich differences in details. In addition, text in CIRR is often complex, which carries semantics that can remain specific when reversed. However, as discussed in Section 4.3, the high complexity of text in CIRR also poses a challenge in the model training, as the text embeddings can be hard to semantically reverse.

5. Conclusion

In this work, we propose a bi-directional training scheme for Composed Image Retrieval that additionally exploits information from the mapping of the (target image, modification text)-pair to the reference image. To tackle the challenge of inferring the reversed semantics of the text with the absence of additional annotations, we leverage the text encoder and prepend learnable tokens to the text inputs. Through finetuning, the text encoder binds the concept of text directionality to said tokens and can produce text embeddings for queries of either direction. We also involve a secondary contrastive loss with a modified sampling strategy for negative samples. We empirically demonstrate that our bi-directional training scheme yields improved performance over a BLIP-based model that has already achieved state-of-the-art performance.

References

- [1] A. Alfassy, L. Karlinsky, A. Aides, J. Shtok, S. Harary, R. Feris, R. Giryes, and A. M. Bronstein. Laso: Label-set operations networks for multi-label few-shot learning. In *2019 IEEE/CVF Conference on Computer Vision and Pattern Recognition (CVPR)*, 2019. 3
- [2] M. U. Anwaar, E. Labintcev, and M. Kleinsteuber. Compositional learning of image-text query for image retrieval. 2021 *IEEE Winter Conference on Applications of Computer Vision (WACV)*, 2020. 1, 2
- [3] A. Baldrati, M. Bertini, T. Uricchio, and A. Del Bimbo. Effective conditioned and composed image retrieval combining clip-based features. In *Proceedings of the IEEE/CVF Conference on Computer Vision and Pattern Recognition (CVPR)*, 2022. 1, 2, 4, 6
- [4] A. Baldrati, M. Bertini, T. Uricchio, and A. Del Bimbo. Conditioned and composed image retrieval combining and partially fine-tuning clip-based features. In *Proceedings of the IEEE/CVF Conference on Computer Vision and Pattern Recognition (CVPR) Workshops*, 2022. 2, 4, 5, 6, 11
- [5] T. L. Berg, A. C. Berg, and J. Shih. Automatic attribute discovery and characterization from noisy web data. In *European Conference on Computer Vision*, 2010. 2
- [6] Y. Chen, S. Gong, and L. Bazzani. Image search with text feedback by visiolinguistic attention learning. In *IEEE Conference on Computer Vision and Pattern Recognition*, 2020. 1, 2, 6
- [7] G. Delmas, R. S. de Rezende, G. Csurka, and D. Larlus. Artemis: Attention-based retrieval with text-explicit matching and implicit similarity. In *International Conference on Learning Representations*, 2022. 2, 6
- [8] E. Dodds, J. Culpepper, S. Herdade, Y. Zhang, and K. Boakye. Modality-agnostic attention fusion for visual search with text feedback. *ArXiv*, abs/2007.00145, 2020. 1, 2, 6
- [9] X. Guo, H. Wu, Y. Gao, S. J. Rennie, and R. Feris. The Fashion IQ Dataset: Retrieving images by combining side information and relative natural language feedback. *ArXiv*, abs/1905.12794, 2019. 1, 2, 5, 6
- [10] X. Han, Z. Wu, P. X. Huang, X. Zhang, M. Zhu, Y. Li, Y. Zhao, and L. S. Davis. Automatic spatially-aware fashion concept discovery. In *IEEE International Conference on Computer Vision*, 2017. 2
- [11] P. Isola, J. J. Lim, and E. H. Adelson. Discovering states and transformations in image collections. In *CVPR*, 2015. 2
- [12] S. Jandial, P. Badjatiya, P. Chawla, A. Chopra, M. Sarkar, and B. Krishnamurthy. Sac: Semantic attention composition for text-conditioned image retrieval. In *2022 IEEE/CVF Winter Conference on Applications of Computer Vision (WACV)*. IEEE Computer Society, 2022. 6
- [13] J. Johnson, B. Hariharan, L. van der Maaten, L. Fei-Fei, C. L. Zitnick, and R. Girshick. Clevr: A diagnostic dataset for compositional language and elementary visual reasoning. In *CVPR*, 2017. 2
- [14] J. Kim, Y. Yu, H. Kim, and G. Kim. Dual Compositional Learning in Interactive Image Retrieval. In *AAAI*, 2021. 2, 6
- [15] J.-H. Kim, S.-W. Lee, D. Kwak, M.-O. Heo, J. Kim, J.-W. Ha, and B.-T. Zhang. Multimodal residual learning for visual qa. In *Advances in neural information processing systems*, 2016. 6
- [16] S.-M. Lee, D. Kim, and B. Han. Cosmo: Content-style modulation for image retrieval with text feedback. 2021 *IEEE/CVF Conference on Computer Vision and Pattern Recognition (CVPR)*, 2021. 6
- [17] B. Lester, R. Al-Rfou, and N. Constant. The power of scale for parameter-efficient prompt tuning. In *Proceedings of the 2021 Conference on Empirical Methods in Natural Language Processing*, 2021. 3
- [18] J. Li, D. Li, C. Xiong, and S. Hoi. Blip: Bootstrapping language-image pre-training for unified vision-language understanding and generation. In *ICML*, 2022. 4, 5, 6
- [19] W. Li, L. Duan, D. Xu, and I. W. Tsang. Text-based image retrieval using progressive multi-instance learning. In *IEEE International Conference on Computer Vision*, 2011. 1
- [20] X. Li, X. Yin, C. Li, X. Hu, P. Zhang, L. Zhang, L. Wang, H. Hu, L. Dong, F. Wei, Y. Choi, and J. Gao. Oscar: Object-semantics aligned pre-training for vision-language tasks. In *European Conference on Computer Vision*, 2020. 5
- [21] Z. Liu, C. Rodriguez, D. Teney, and S. Gould. Image retrieval on real-life images with pre-trained vision-and-language models. In *IEEE International Conference on Computer Vision*, 2021. 1, 2, 5, 6, 7, 8, 11
- [22] I. Loshchilov and F. Hutter. Decoupled weight decay regularization. In *International Conference on Learning Representations*, 2017. 5
- [23] P. Micikevicius, S. Narang, J. Alben, G. Diamos, E. Elsen, D. Garcia, B. Ginsburg, M. Houston, O. Kuchaiev, G. Venkatesh, and H. Wu. Mixed precision training, 2017. 6
- [24] E. Perez, F. Strub, H. de Vries, V. Dumoulin, and A. Courville. Film: Visual reasoning with a general conditioning layer, 2017. 6
- [25] A. Radford, J. W. Kim, C. Hallacy, A. Ramesh, G. Goh, S. Agarwal, G. Sastry, A. Askell, P. Mishkin, J. Clark, G. Krueger, and I. Sutskever. Learning transferable visual models from natural language supervision. In *Proceedings of the 38th International Conference on Machine Learning*, 2021. 2, 4
- [26] N. Ruiz, Y. Li, V. Jampani, Y. Pritch, M. Rubinstein, and K. Aberman. Dreambooth: Fine tuning text-to-image diffusion models for subject-driven generation. In *arXiv preprint arxiv:2208.12242*, 2022. 2, 3
- [27] K. Saito, K. Sohn, X. Zhang, C.-L. Li, C.-Y. Lee, K. Saenko, and T. Pfister. Pic2word: Mapping pictures to words for zero-shot composed image retrieval. *ArXiv*, 2023. 1, 2
- [28] A. Santoro, D. Raposo, D. G. Barrett, M. Malinowski, R. Pascanu, P. Battaglia, and T. Lillicrap. A simple neural network module for relational reasoning. In *Advances in neural information processing systems*, pages 4967–4976, 2017. 6
- [29] C. Schuhmann, R. Beaumont, R. Vencu, C. W. Gordon, R. Wightman, M. Cherti, T. Coombes, A. Katta, C. Mullis, M. Wortsman, P. Schramowski, S. R. Kundurthy, K. Crownson, L. Schmidt, R. Kaczmarczyk, and J. Jitsev. LAION-5b: An open large-scale dataset for training next generation

image-text models. In *Thirty-sixth Conference on Neural Information Processing Systems Datasets and Benchmarks Track*, 2022. 5

- [30] M. Shah, X. Chen, M. Rohrbach, and D. Parikh. Cycle-consistency for robust visual question answering. In *2019 Conference on Computer Vision and Pattern Recognition (CVPR)*. IEEE, 2019. 3
- [31] A. Suhr, S. Zhou, A. Zhang, I. Zhang, H. Bai, and Y. Artzi. A corpus for reasoning about natural language grounded in photographs. *Proceedings of the 57th Annual Meeting of the Association for Computational Linguistics*, 2019. 5
- [32] C. Szegedy, V. Vanhoucke, S. Ioffe, J. Shlens, and Z. Wojna. Rethinking the inception architecture for computer vision. In *2016 IEEE Conference on Computer Vision and Pattern Recognition (CVPR)*, 2016. 5
- [33] S. Tong and E. Chang. Support Vector Machine active learning for image retrieval. In *Proceedings of the Ninth ACM International Conference on Multimedia*, 2001. 1
- [34] A. Vaswani, N. Shazeer, N. Parmar, J. Uszkoreit, L. Jones, A. N. Gomez, u. Kaiser, and I. Polosukhin. Attention is all you need. In *International Conference on Neural Information Processing Systems*, 2017. 5
- [35] N. Vo, L. Jiang, C. Sun, K. Murphy, L.-J. Li, L. Fei-Fei, and J. Hays. Composing text and image for image retrieval - an empirical odyssey. In *IEEE Conference on Computer Vision and Pattern Recognition*, 2019. 1, 2, 3, 5, 6
- [36] Y. Yu, S. Lee, Y. cheol Choi, and G. Kim. Curlingnet: Compositional learning between images and text for fashion iq data. *ArXiv*, 2020. 2, 6
- [37] C. Zhang, J. Y. Chai, and R. Jin. User term feedback in interactive text-based image retrieval. *Proceedings of the 28th Annual International ACM SIGIR Conference on Research and Development in Information Retrieval*, 2005. 1
- [38] H. Zhu, Y. Wei, Y. Zhao, C. Zhang, and S. Huang. Amc: Adaptive multi-expert collaborative network for text-guided image retrieval. *ACM Trans. Multimedia Comput. Commun. Appl.*, 2023. 6
- [39] J.-Y. Zhu, T. Park, P. Isola, and A. A. Efros. Unpaired image-to-image translation using cycle-consistent adversarial networks. In *Computer Vision (ICCV), 2017 IEEE International Conference on*, 2017. 3

Supplementary Material

A. Implementation Details

Balancing the Reversed Loss. Here we provide details on determining the hyperparameter α in the loss mentioned in Equation 3. As discussed in Section 3.3, due to the false negative issue in the reversed path, the magnitude of the reversed loss term \mathcal{L}_B is generally higher, and one shall pay special attention to balancing it with the forward loss term \mathcal{L}_F such that the reversed queries do not inadvertently harm the training. We also note that the second-stage combiner training is more sensitive to tunings in α compared to the first stage. We suspect the reason to be related to the model capacity, as the first-stage finetuning is relatively light in architecture, while the second-stage combiner module is of much higher complexity (Figure 2). To this end, the combiner could more easily, and quickly, overfit the noise brought by the false negatives.

Table 4 lists the α values used in our training on both datasets. We conduct a grid search to identify the optimal α . For Fashion-IQ, in both stages, we discover that an α of around 0.5 is optimal, while for the first stage, further decreasing it to 0.4 yields slightly better results. On CIRR, we find that the training consistently benefits from a relatively small α .

	Fashion-IQ		CIRR	
	Stage-I	Stage-II	Stage-I	Stage-II
α	0.4	0.5	0.1	0.1

Table 4. α values used in our experiments.

B. Inference on Reversed Queries

Section 3.3 details the impact of false-negatives. In Table 5 we demonstrate that validating on the reversed queries yields subpar results, which collaborates with our observation of a higher loss in the reversed path. This leads to our inference strategy that only takes into account the forward queries.

C. Recall_{Subset} on CIRR

As mentioned in Section 4.2, we notice that the state-of-the-art architecture (i.e., combiner [4]) learns poorly on the more challenging Recall_{Subset} $@K$ metric. Here, we illustrate its performance on Recall_{Subset} $@1$ throughout training. As shown in Figure 5 left (blue), the combiner effectively fails in learning on said metric, with the performance gradually decreasing. We also note the high fluctuations observed among epochs, which is partially due to the high granularity of the metric (as discussed in Section 4.2). To compare, we overlay the validation curve obtained using our

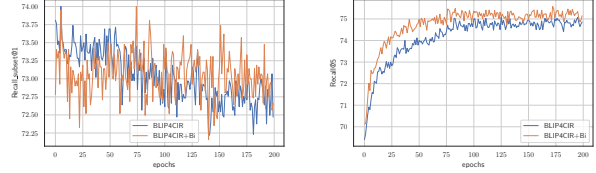


Figure 5. Validation performance on (left) Recall_{Subset} $@1$ and (right) Recall $@5$ throughout training (200 epochs). Results obtained on the CIRR validation set. **BLIP4CIR**: baseline model that uses combiner architecture. **BLIP4CIR+Bi**: our method that involves the bi-directional training scheme.

bi-directional training scheme, as in Figure 5 left (orange). We note that globally, our performance in Recall_{Subset} $@1$ is on par with the baseline. However, since we follow previous work [21] to select the best-performing epoch via an average score of Recall $@5$ and Recall_{Subset} $@1$, the reported performance in Table 2 and Table 3 may not necessarily be optimal on each individual metric.

We stress that our bi-directional training scheme does *not* aim at improving the existing model architecture. Hence, it is unsurprising that our method inherits the issues on Recall_{Subset} $@K$ from the combiner baseline. Given the characteristics of the validation curves, we argue that the performance comparison between the baseline and our method on Recall_{Subset} $@K$ (Table 2) shows little insight. We instead point to other metrics, such as Recall $@5$ or 10 for comparison, as discussed in Section 4.2. As an example, we showcase the validation curve on Recall $@5$ through training (Figure 5 right).

		Fashion-IQ			CIRR			
BLIP4CIR+Bi		R@10	R@50	Average	R@1	R@5	R _{Subset} @1	Average
1	on forward queries	43.49	67.31	55.40	42.36	75.46	72.90	74.18
2	on reversed queries	23.08	45.05	34.07	18.08	49.25	44.51	46.88

Table 5. Comparison of performance when validating on the forward and reversed queries. Results obtained on validation sets, as in Table 3.